The Journal of Clinical Endocrinology & Metabolism, 2024, **00**, 1–13
https://doi.org/10.1210/clinem/dgae839
Advance access publication 6 December 2024
Clinical Research Article

Out-of-frame Translation Rescues a Loss-of-function Variant in a Novel *TBCE* Phenotype

Peter Sparber,[1] Evgeniia Ulas,[2,3] Alexandra Filatova,[1] Eugene Tatarskiy,[1] Grigory Perelman,[1] Nina Makretskaya,[1] Elena Nagaeva,[4] Maria Kareva,[4] Elena Frolova,[5] Natalia Kalinchenko,[4] Anna V. Tvorogova,[6] Sergey Golyshev,[3] Anton Burakov,[3] Vyacheslav Tabakov,[1] Ekaterina Lozier,[7] Fedor Konovalov,[7] Victoria Voinova,[8] Anatoly Tiulpakov,[1] and Mikhail Skoblov[1]

[1]Department of Functional Genomics, Research Centre for Medical Genetics, 115478 Moscow, Russian Federation
[2]Department of Cell Biology, Institute of Protein Research of Russian Academy of Science, 142290 Moscow, Russian Federation
[3]A.N. Belozersky Institute of Physico-Chemical Biology, Lomonosov Moscow State University, 119992 Moscow, Russian Federation
[4]Institute of Pediatric Endocrinology, Endocrinology Research Centre, 117292 Moscow, Russian Federation
[5]Consulting and Diagnostic Department, National Medical Research Center for Children's Health Federal State Autonomous Institution of the Russian Federation Ministry of Health, 119991 Moscow, Russian Federation
[6]Center for Precision Genome Editing and Genetic Technologies for Biomedicine, Institute of Gene Biology, Russian Academy of Sciences, 119334 Moscow, Russian Federation
[7]Independent Clinical Bioinformatics Laboratory, Moscow, Russian Federation
[8]Clinical Genetics Department, Veltischev Research and Clinical Institute for Pediatrics Pirogov RNRMU, 125412 Moscow, Russian Federation

Correspondence: Peter Sparber, PhD, Research Centre for Medical Genetics, Moskvorechie St 1, 115478 Moscow, Russian Federation. Email: psparber93@gmail.com.

Abstract

Context: Pathogenic variants in the *TBCE* gene, encoding tubulin-specific chaperone E crucial for tubulin folding, are linked to three severe neurodevelopmental disorders: Hypoparathyroidism-retardation-dysmorphism syndrome, Kenny-Caffey syndrome type 1, and progressive encephalopathy with amyotrophy and optic atrophy.

Objective: We identified patients with a novel, milder *TBCE*-associated phenotype and aimed to characterize it at the clinical and molecular levels.

Materials and Methods: We conducted splicing analysis using deep next-generation sequencing of RT-PCR products and detected TBCE through Western blotting. Translation efficiency was measured using a luciferase reporter assay. Overexpression experiments were performed in Hela cells with tubulin staining. Immunofluorescence analysis was used for Golgi complex assessment, while microtubule dynamics were studied post-nocodazole treatment. Electron microscopy facilitated ultrastructural studies.

Results: We report 7 patients with a novel, milder *TBCE* phenotype, presenting with amyotrophy, testicular failure, and mild intellectual disability, with or without short stature. All patients were homozygous or compound-heterozygous for the NM_003193.5:c.100 + 1G > A variant, which causes a splicing alteration and early frameshift. However, we found that the mild phenotype arises due to translation from an alternative open reading frame, producing a partially functional protein. Dermal fibroblasts showed reduced Golgi compactness but normal microtubule dynamics. Electron microscopy revealed varying levels of acto-myosin degradation. The c.100 + 1G > A variant was found to be 10 times more frequent in Slavic samples than in gnomAD, suggesting underdiagnosis of this phenotype.

Conclusion: This study uncovers complex molecular mechanisms contributing to the milder phenotype in patients with the c.100 + 1G > A variant, providing insights into a new *TBCE*-related disorder.

Key Words: TBCE, tubulin-specific chaperone E, splicing, out-of-frame translation, microtubule, tubulin, new phenotype

Microtubules (MTs) are essential components of the cell cytoskeleton, formed by the polymerization of α and β-tubulin heterodimer molecules (1). MTs play a critical role in maintaining cellular shape and structure, essential for correct cell division (2), intercellular transport (3), and many other pivotal cellular mechanisms. The assembly and disassembly of MTs are highly dynamic, and they can spontaneously alternate these phases in a process referred to as dynamic instability (4).

The proteostasis of tubulin heterodimers is regulated by a complex interplay of several MT-associated proteins, including the cytosolic chaperonin complex CCT, the co-chaperone complex prefoldin, the small Arl2 GTPase, and 5 tubulin-binding cofactors (TBCs): TBCA, TBCB, TBCC, TBCD, and TBCE (5, 6). TBCB binds the near-native form of α-tubulin after its CCT-mediated folding (7), while TBCA binds nascent β-tubulin. Subsequently, TBCB and TBCA are replaced by TBCE and TBCD, respectively. TBCC then drives TBCE-α-tubulin and TBCD-β-tubulin to form a protein complex consisting of α-tubulin, β-tubulin, TBCC, TBCD, and TBCE. TBCC also activates Arl2 GTP hydrolysis in a parallel

Received: 19 September 2024. **Editorial Decision:** 26 November 2024. **Corrected and Typeset:** 19 December 2024

pathway, leading to the formation of native αβ-tubulin heterodimers (8). Additionally, TBCE and TBCB can dissociate αβ-tubulin heterodimers by sequestering α-tubulin monomers and forming an α-tubulin-TBCE-TBCB complex, thereby regulating MT dynamics by changing of free αβ-tubulin heterodimers concentration. Overexpression of TBCE completely disrupts the cell MT network (9). The TBCE protein consists of 527 amino acids and contains an N-terminal cytoskeleton-associated protein glycine-rich (CAP-Gly) domain, which mediates α-tubulin specific interaction, followed by leucine-rich repeat (LRR) domains and a C-terminal ubiquitin-like domain, possibly involved in α-tubulin degradation via the proteasome.

Pathogenic variants in the *TBCE* gene are associated with 3 extremely rare, severe neurodevelopmental phenotypes with autosomal recessive inheritance: hypoparathyroidism-retardation-dysmorphism (HRD) syndrome, characterized by extreme growth failure, congenital hypoparathyroidism, severe intellectual disability, and facial dysmorphism; Kenny-Caffey syndrome type 1, which partially overlaps with HRD syndrome and includes osteosclerosis and medullary stenosis as additional features (10); and a distinct phenotype described as progressive encephalopathy with amyotrophy and optic atrophy (11). The first 2 phenotypes have been almost exclusively reported in patients with Middle Eastern ancestry, with the in-frame deletion c.155_166del found in a homozygous state in all patients. HRD was additionally described in a Belgian pedigree with 2 affected siblings carrying a 2 bp deletion in exon 1 (c.66_67del) and a nonsense variant in exon 12 (c.1113T > A) in a compound heterozygous state (10). In the progressive encephalopathy with amyotrophy and optic atrophy phenotype, 6 patients originating from Italy all shared the c.464T > A missense variant in a homozygous or compound heterozygous state, which was suggested to have a hypomorphic effect.

As TBCE is an essential component of the MT assembly machinery; complete absence of the protein is assumed to be lethal. In mice, a homozygous knockout of *TBCE* leads to preweaning lethality with complete penetrance (MGI:5588279). This observation contradicts the presence of patients harboring 2 loss-of-function (LoF) variants in the Belgian HRD family. However, in the work of Tian et al, it was demonstrated that a functional TBCE protein is translated from the c.66_67del allele due to a cryptic translation from 3 downstream out-of-frame ATG codons, thus resolving this paradox (12).

Here we describe 7 patients with a novel, milder *TBCE*-associated phenotype. All patients carry the NM_003193.5:c.100 + 1G > A variant in a homozygous or compound heterozygous state. Extensive phenotyping revealed that amyotrophy, testicular failure, and mild intellectual disability with or without short stature are the main features of this new phenotype. Detailed molecular and cellular characterization demonstrated that although c.100 + 1G > A leads to a presumed complete LoF by disrupting splicing, cryptic translation rescues tubulin formation in these patients. We show that the reduced translation level of the mutant TBCE is associated with both reduced stability of the altered N-terminus and competition for ribosome binding with the reference ATG start codon. At the cellular level, we observed partial overlap with previously reported *TBCE* phenotypes with reduced compactness of the Golgi complex and increased number of large electrolucent vacuoles in patient fibroblasts. By comparing with other data, we deciphered the molecular consequences of different *TBCE*-associated variants and mapped the core region of the CAP-Gly domain that is sufficient for α-tubulin binding, thus providing new insights into the biology of TBCE functioning.

Materials and Methods

Detailed materials and methods can be found in the Supplementary Materials and Methods file (13) and describe the following: variant nomenclature, subjects, bioinformatic analysis, genetic analysis, RT-PCR, targeted next generation sequencing of RT-PCR products, luciferase reporter assay, Western blotting, TBCE overexpression, microtubule regrowth assay and immunofluorescence microscopy, fibroblast motility analysis, electron microscopy, and statistical analysis.

All research participants gave written informed consent (or responsible consent form for infant proband) to the clinical examination and the publication of their anonymized data. Additionally, the 3 participants whose photographs appear in the manuscript provided responsible consent for the publication of their images.

Results

Clinical Description and Genetic Diagnosis

The study included 7 patients from 6 unrelated Slavic families of Russian origin, consisting of 6 males and 1 female. Detailed clinical information regarding all 7 patients can be found in Supplementary Table S1 (13), with individual case presentations included in Supplementary File 2 (13).

One patient initially sought consultation with a clinical geneticist at the age of 14 due to extremely low weight and lack of muscle mass. The remaining patients received counseling from an endocrinologist due to short stature, with 3 patients presenting partial growth hormone (GH) deficiency (patients 3,4,5) and the others showing hypogonadism (Patients 2-1, 2-2, and 6). The mean age at initial presentation was 10.6 years, ranging from 1 month to 18.2 years.

Except for 1 patient, all patients exhibited low body weight with reduced muscle mass, indicated by body mass index SD score ranging from −2.17 to −6.05 (Supplementary Table S1) (13). During clinical examination, mild facial dysmorphic features were noted in all subjects, including large protruding ears, micrognathia, and a triangular face. Narrow shoulders, narrow waist, long neck, and lumbar scoliosis were also observed. The patients displayed amyotrophy due to muscle wasting, which was determined not to be caused by neurogenic changes based on electromyography results (Fig. 1). Additionally, all patients displayed signs of mild intellectual disability that was characterized by reduced adaptive functioning, which resulted in tailored support from their caregivers, unawareness of their physical condition, and academic struggling that required remedial education.

In pubertal-aged male patients, hormone profiling confirmed the diagnosis of hypergonadotropic hypogonadism, indicated by increased serum levels of FSH and LH. They all exhibited reduced testis volume, which, strikingly, did not correspond to the advanced genital and pubic Tanner staging. In addition, testicular microlithiasis was observed during ultrasound examinations (Supplementary Table S1) (13). In the only female patient, levels of gonadotropins were within normal range and pelvic ultrasound showed normal sizes of

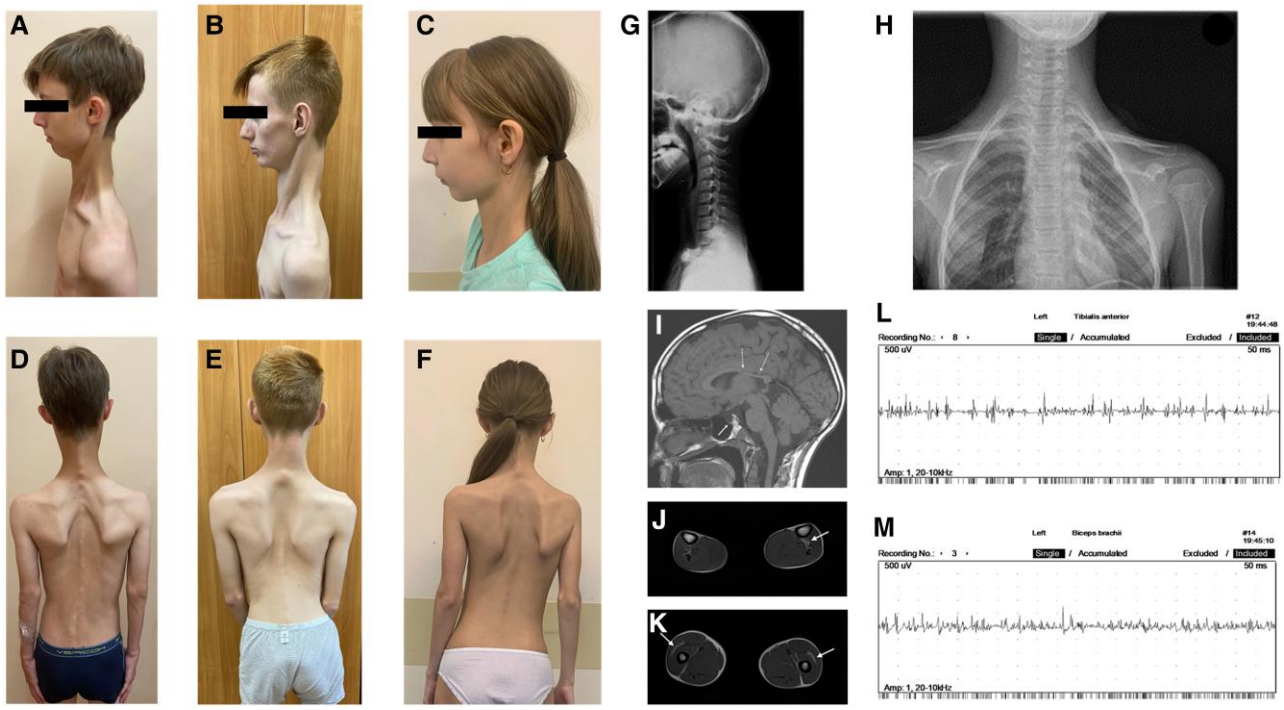

Figure 1. Clinical features of patients with amyotrophy, testicular failure, and mild intellectual disability with or without short stature. (A-F) Phenotype of patient 3 (A, D), patient 1 (B, E), and patient 5 (C, F) showing extremely reduced body weight, atrophy of the paravertebral muscles, long neck, scoliosis, and mild facial dysmorphic features. (G, H) X-ray of patient 3 with cervicalization of thoracic vertebrae and thoracic scoliosis. (I) Sagittal MRI of patient 3 in T1-weighted image. White arrows indicate hypoplasia of the corpus callosum and partial empty sella syndrome. (J, K) Lower limb muscle MRI in T1-weighted image of patient 1 with involvement of m. vastus intermedius and m. tibialis posterior indicated with white arrows. (L, M) Electromyography of n. tibialis anterior and n. biceps brachii of patient 1 displaying signs of myopathic changes.

Abbreviation: MRI, magnetic resonance imaging.

the uterus and ovaries. But she was examined during puberty development (Tanner stage 3-4), and she only started to have her menstrual cycles. At the time of molecular diagnosis, none of the patients exhibited clinical or laboratory signs (where available) consistent with hypoparathyroidism, although transient hypocalcemia was reported during the first month of life in patient 3, with normal levels of calcium, phosphate, and PTH observed later in life (Supplementary Table S1) (13).

Brain magnetic resonance imaging (MRI) was performed in 6 out of 7 patients, revealing pituitary hypoplasia in 3 cases and hypoplasia of the corpus callosum in 2 cases. In 2 patients, brain MRI results were considered normal. Overall, the patient cohort exhibited a distinct phenotype characterized by amyotrophy, testicular failure, and mild intellectual disability with or without short stature.

Whole-exome sequencing (WES) was performed on 5 patients, but no potentially causative variants were detected in genes associated with known endocrine or neuromuscular disorders. However, all 5 patients exhibited the c.100 + 1G > A variant in the *TBCE* gene, either in a homozygous state (3 patients) or a compound heterozygous state. In patient 2-2, the same variant was identified in a homozygous state through Sanger sequencing after WES analysis of his younger brother. Additionally, targeted analysis for the c.100 + 1G > A variant was performed on patient 5 due to high phenotypic similarity with other patients in the cohort. Once again, the c.100 + 1G > A variant was detected in a homozygous state, confirming that the reported phenotype can be distinguished clinically.

This variant has been reported several times in ClinVar with conflicting interpretations of pathogenicity. The c.100 + 1G > A variant is located at the highly conserved donor splice site dinucleotide of intron 2 and is predicted to disrupt splicing by SpliceAI with a Δ score of DL—1.00 and DG—0.96 and activation of a cryptic donor site in exon 2 34 nucleotide upstream (Supplementary Fig. S1) (13). The variant was found in 109 alleles in gnomAD v4.2.1 in a heterozygous state, predominantly in samples of European (non-Finnish) ancestry, with no homozygotes reported. According to the American College of Medical Genetics guidelines, the variant has been classified as likely pathogenic (PVS1, PM2) (14).

Patient 6 was compound heterozygous for the c.100 + 1G > A variant and the c.101G > T [p.(Gly34Val)] missense variant in the *TBCE* gene. The missense variant was previously described in trans position with a LoF variant in a patient with epilepsy (15). This variant is located at a conserved amino acid residue in the CAP-Gly domain, crucial for tubulin binding. Moreover, it changes the first nucleotide of exon 3, which can disrupt splicing by affecting critical exonic cis-regulatory sequences (16). SpliceAI predicted that the c.101G > T variant leads to acceptor loss with a Δ score of 0.26 (Supplementary Fig. S2) (13). Overall, this variant has been classified as likely pathogenic (PM2, PP3, PM1, PM3, PP5).

In patient 3, along with the c.100 + 1G > A variant, a novel missense variant, c.512T > A [p.(Val171Glu)], was observed at the end of the LRR1 domain. Based on the high similarity of the patient's phenotype to other reported cases and the predicted deleterious effect by in silico tools, this variant has also been classified as likely pathogenic (PM2, PP3, PM3, PP4).

Biallelic variants in the *TBCE* gene are associated with 3 distinct phenotypes: HRD, Kenny-Caffey syndrome type 1, and progressive encephalopathy with amyotrophy and optic atrophy. However, the patients in our study did not exhibit

Table 1. Comparison of the main symptoms of known and newly described TBCE-associated phenotype

Feature/phenotype	Amyotrophy, testicular failure, intellectual disability with or without short stature	Progressive encephalopathy with amyotrophy and optic atrophy	Hypoparathyroidism-retardation-dysmorphism syndrome	Kenny–Caffey syndrome type 1
Genotype	**c.100 + 1G > A homozygous (5/7); c.100 + 1G > A compound heterozygous (2/7)**	**c.464T > A homozygous (⅝); c.464T > A compound heterozygous (⅛)**	**c.155_166del homozygous; c.66_67del/c.1113T > A**	**c.155_166del homozygous**
Low birth weight/ length	–/+	–	+	+
Short stature	–/+	–	+	+
Facial dysmorphism	+	–	+	+
Amyotrophy	+	+	–	–
Optic atrophy	–	+	–	–
Intellectual disability	Mild	Mild to severe	Severe	No/severe
Hypoparathyroidism	–	–	+	+
Hypogonadism	+	–	+	–
GH deficiency	–/+	n/a	–/+	n/a
Recurrent infections	–	–	+	+
Osteosclerosis	–	–	–	+
Medullary stenosis	–	–	–	+
Brain MRI	Hypoplasia of the adenohypophysis (2/6*), hypoplasia of corpus callosum (2/6*)	Hypoplasia of corpus callosum, cerebellar atrophy, iron accumulation in GP and SN (in some patients in the second decade)	Hypoplasia of the adenohypophysis, hypoplasia of corpus callosum, decreased white matter volume, delayed myelination	n/a
Overall severity	+	++	+++	+++

Asterisks indicate missing data. All variants are named according to the recommendations of the Human Genome Variation Society. The nucleotide changes are described based on the mRNA isoform NM_003193.5.
Abbreviations: GH, growth hormone; GP, globus pallidus; MRI, magnetic resonance imaging; n/a - not available; SN, substantia nigra.

signs of congenital hypoparathyroidism, extreme growth failure, severe intellectual disability, recurrent infections, osteosclerosis, or medullary stenosis, which are characteristic features of HRD and Kenny-Caffey syndrome type 1. Although amyotrophy was diagnosed in all our patients, it did not originate from a neurogenic cause, as seen in progressive encephalopathy with amyotrophy and optic atrophy syndrome, which typically presents with signs of distal motor neuropathy resembling distal spinal muscular atrophy. Additionally, careful monitoring of several patients revealed no signs of disease progression, and there were no reported changes in vision among the subjects. An exception was Patient 6 (c.100 + 1G > A/c.101G > T), who lost ambulation during the disease course due to severe muscular hypotonia.

Considering the overall phenotype in our patient cohort compared to previously reported cases (Table 1) and based on the identification of a high-confidence LoF variant, all evidence strongly supports the observation of a new, milder *TBCE*-associated phenotype in our patients.

RT-PCR Coupled With Targeted Next-Generation Sequencing Reveals Loss of Function Effect for the c.100 + 1G > A and c.101G > T Variants

Even though a predicted LoF variant was found in a homozygous state in 5 out of 7 patients and in a compound heterozygous state in the remaining 2, all demonstrated a distinct, milder phenotype compared to what was reported in the literature. To evaluate the effect of the c.100 + 1G > A variant on splicing and explain the phenotypic discrepancy observed in our patients, we performed RT-PCR analysis. Total RNA was extracted from primary dermal fibroblast cultures obtained from forearm biopsy samples from patient 1, his mother (a heterozygous carrier of the investigated variant), and patient 6.

RT-PCR analysis with subsequent Sanger sequencing showed a wild-type (WT) splicing pattern with the inclusion of exons 1-5 in the control sample. In a trace amount, we observed skipping of exon 3, corresponding to the NM_001287802.2 isoform of the *TBCE* gene. In patient 1's mother, we observed 2 isoforms: a long isoform with the WT transcript and a short abnormal isoform. Sanger sequencing of the mutant isoform showed that the c.100 + 1G > A variant leads to both skipping of exon 3 and activation of a cryptic donor splice site in exon 2, confirming SpliceAI prediction (Supplementary Fig. S1) (13). Overall, the splicing alteration led to deletion of 119 nucleotides. At the protein level, such a deletion is predicted to lead to a frameshift and the formation of a premature termination codon early in the mRNA structure (p.Thr33delInsAla62fsTer24). In patient 1's sample, we detected only the mutant isoform without any residual level of WT transcript (Supplementary Fig. S1) (13).

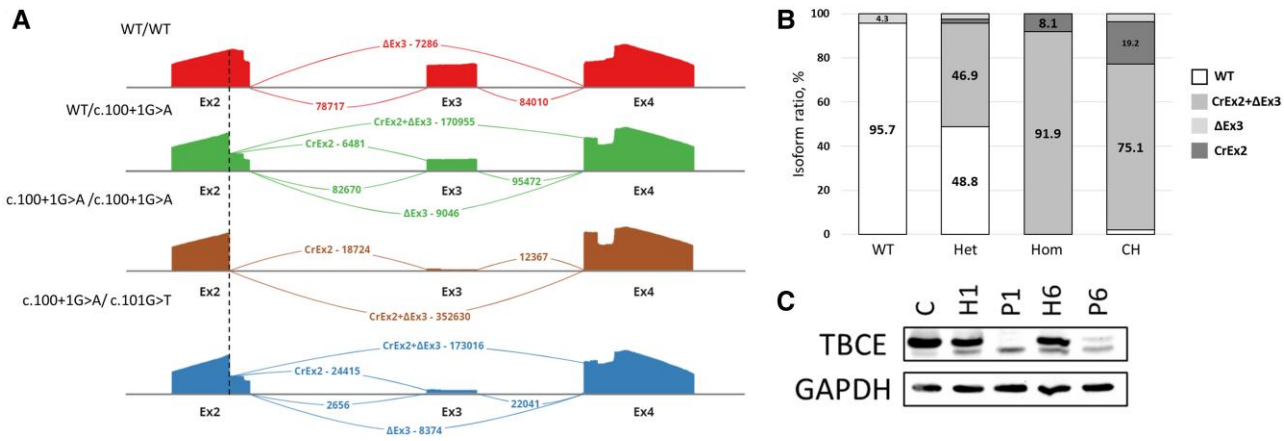

Figure 2. Molecular characterization of the c.100 + 1G > A and c.101G > T variants in the *TBCE* gene. (A) Sashimi plot with exon-exon junction visualization of deep sequencing of RT-PCR products in a control sample (red), a heterozygous carrier of the c.100 + 1G > A variant (green), patient 1 who is homozygous for the c.100 + 1G > A variant (brown), and patient 6, who is compound heterozygous for the c.100 + 1G > A and c.101G > T variants (blue). Numbers indicate the amount of exon-exon junction reads for each isoform. (B) Quantification of different isoform ratios for various genotypes. (C) TBCE Western blot analysis from dermal fibroblasts of a control sample (lane 1), heterozygous carriers of the c.100 + 1G > A variant (lanes 2 and 4), and patients 1 and 6 (lanes 3 and 5, respectively). Glyceraldehyde-3-phosphate dehydrogenase was used for protein normalization.

Abbreviations: CH, compound-heterozygous (patient 6); Het, heterozygous carrier of the c.100 + 1G > A variant; Hom, homozygous (c.100 + 1G > A) (patient 1); WT, wild-type.

The same splicing pattern was detected in a myoblast culture obtained from a muscle biopsy sample of patient 1 (Supplementary Fig. S3) (13). In patient 6's cDNA sample, we observed, along with the short isoform that corresponded to the 119 bp deletion, a longer isoform and partial expression of the WT transcript, confirming the partial splicing change caused by the c.101G > T variant (Supplementary Fig. S2) (13).

To quantitatively analyze different isoform ratios in patients with the c.100 + 1G > A and c.101G > T variants, we performed targeted next-generation sequencing (NGS) of RT-PCR products.

In the control sample, we observed 4.3% skipping of exon 3 with 95.7% normal splicing (Fig. 2A and 2B). In the sample from patient 1's mother (Fig. 2B), 46.9% of all exon-junction reads corresponded to exon 3 skipping and activation of a cryptic exon 2, as observed on RT-PCR. Additionally, trace amounts of skipping of exon 3 and isolated activation of the cryptic donor site in exon 2 were observed (2.5% and 1.8%, respectively) (Fig. 2A and 2B).

In patient 1 (Fig. 2B), 91.9% of all exon-junction reads corresponded to the abnormal isoform previously found on RT-PCR, and in 8.1%, activation of the cryptic donor site with inclusion of exon 3 was observed (Fig. 2A and 2B). In patient 6 (CH, Fig. 2B), the majority of transcripts (94.3%) corresponded to the splicing alteration caused by the c.100 + 1G > A variant. An isoform with isolated exon 3 skipping caused by the c.101G > T variant was found in only 3.6% suggesting that this isoform is degraded by the nonsense-mediated decay (NMD) machinery. This is further confirmed by the allelic ratio of the c.101G > T variant in exon 3, which significantly skewed toward the G allele (Supplementary Fig. S4) (13). Overall, the WT splicing pattern was observed in patient 6 in only 2.1% of exon-junction reads (Fig. 2A and B) explaining his more severe clinical phenotype.

Given the fact that we observed a 50:50 ratio between the WT and the abnormal isoform in a heterozygous carrier of the c.100 + 1G > A variant and since no inhibition of NMD was performed, we conclude that the mutant isoform caused by the c.100 + 1G > A variant is translated into a short protein lacking all TBCE domains and therefore could not be functional.

Cryptic Translation Restores the Reading Frame and Produces a Shortened Mutant TBCE Protein

No patients with complete absence of TBCE are reported in the literature. Moreover, according to Mouse Genome Informatics (MGI), a *TBCE* homozygous knockout is associated with a preweaning lethality phenotype with complete penetrance (MGI:5588279). Since RT-PCR coupled with deep NGS sequencing of cDNA results contradicted the observation of a relatively mild clinical phenotype in our patients, we hypothesized that the explanation may be related to the translation process of the mutant TBCE protein.

Previously, it was shown that the first coding exon of *TBCE* contains 3 additional ATG codons in the +1 frame, and translation can be initiated from any of them. This cryptic translation was demonstrated to rescue tubulin formation, leading to a functional TBCE protein in an HRD patient with a 2 bp deletion in exon 2 (c.66_67del) (12). To explore the possibility of a similar mechanism in our patients, we performed bioinformatic analysis of possible cryptic translation in the mutant *TBCE* mRNA isoform observed by RT-PCR analysis in patient 1.

Analysis using both ATGpr_sim and ORFfinder predicted translation from the +1 frame starting from the first downstream ATG codon, resulting in a 480 amino acid long protein (compared to 527 in WT). In the +1 frame, the first 2 codons encode the same amino acids as in the WT protein, followed by 13 different amino acids. The cryptic translation starts from a frame shifted by 1 nucleotide compared to WT. The 119-nucleotide deletion of exon 3 and part of exon 2 also shifts the reading frame by one nucleotide, resulting in identical sequences starting from exon 4 in both WT and mutant *TBCE*. Overall, bioinformatic analysis predicted the formation of a slightly shorter TBCE protein with a different N-terminus and partial deletion of the CAP-Gly domain,

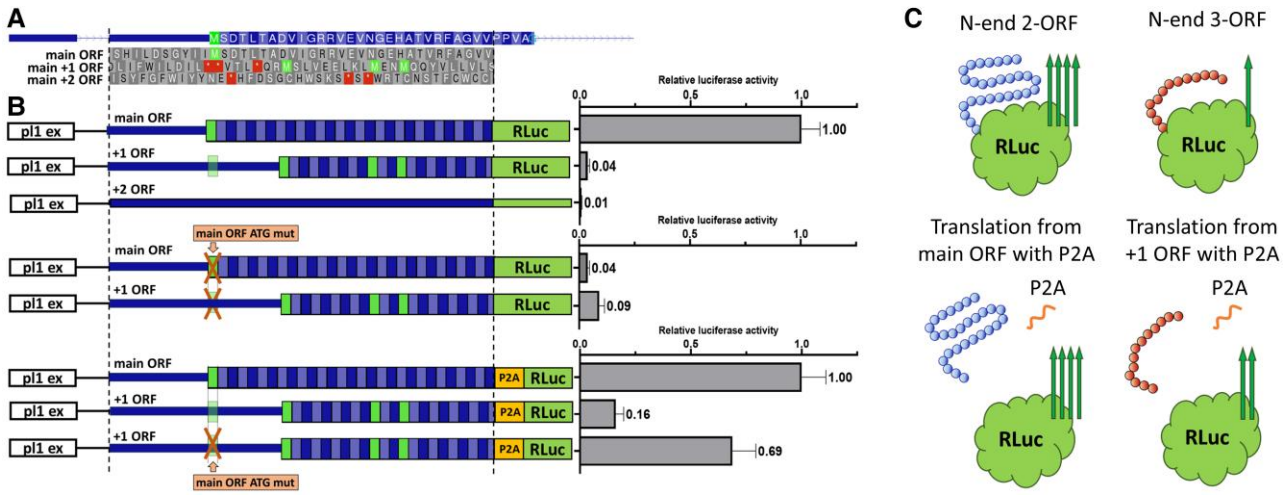

Figure 3. Ribosomal competition and reduced protein stability due to altered N-end affect translation efficiency from out-of-frame ATG codons in the *TBCE* gene. (A) Structure of the first coding exon of the *TBCE* gene (exon 2) with all 3 reading frames located below. Start codons are indicated by a green square. Cryptic translation initiates from the +1 ORF. (B) Quantification of translation efficiency using a luciferase assay. Upper panel: Translation efficiency of +1 ORF compared with the main ORF under wild-type conditions. Translation efficiency from the +2 ORF indicates translational background. Middle panel: the effect of the main ORF ATG codon on the translation efficiency of +1 ORF (details in text). Lower panel: the effect of the altered N-end on the translation efficiency of the +1 ORF (middle part) and the influence of both the main ORF and altered N-end on +1 ORF translation efficiency (lower part, details in text). In all cases, mean relative luciferase activity was measured from at least 3 biological replicates. Error bars indicate ± SE of the mean. (C) Schematic representation of the influence of the TBCE-altered N-end on luciferase activity. Removal of the altered N-end by P2A-mediated "cleavage" leads to an increase in luciferase activity.

Abbreviation: ORF, open reading frame.

with only the last 10 amino acids present in the mutant protein (Supplementary Fig. S1) (13).

Western blot analysis performed on patient 1 fibroblast lysates confirmed the translation of a small amount of a shorter TBCE protein (Fig. 2C, lane 3). In patient 6 samples, in agreement with the RT-PCR results, a shortened TBCE isoform was observed along with residual levels of full-length TBCE (Fig. 2C, lane 5).

Quantification of Translation Efficiency

To analyze the translation initiation potential of different *TBCE* open reading frames, we performed a luciferase assay. We cloned a segment of *TBCE* exon 2 corresponding to the shortened isoform resulting from the splicing change due to the c.100 + 1G > A variant. We created 3 separate luciferase constructs with this exon fused with *Renilla* luciferase open reading frame in 1 of the 3 possible frames (Fig. 3A). The main ORF that normally produces the TBCE protein, starts with a single ATG codon in a Kozak sequence with moderate strength. The +1 ORF that contains 3 downstream ATG codons that can produce a truncated TBCE protein from an aberrant isoform caused by the c.100 + 1G > A variant. + 2 ORF does not contain any ATG codons and is unlikely to be translated. We used the +2 frame as a background control for the luciferase assay.

We transfected these 3 luciferase plasmids into the HEK293T cell line and measured their relative luciferase activities 48 hours after transfection. We observed that the translation efficiency of the +1 ORF is only ~4% of the translation level of the main ORF (adjusted *P*-value < .0001), while the translation background (+2 ORF) is less than 1% (adjusted *P*-value < .0001) (Fig. 3B). Thus, we concluded that translation of the truncated TBCE protein from the aberrant mRNA isoform is present but at a very low level. This finding is consistent with the Western blot analysis of patient fibroblasts and with previously published data (12).

Despite the fact that the +1 ORF contains 3 ATG codons, 2 of which are in a more optimal Kozak context than the reference start codon, it produces a significantly lower amount of protein compared to the reference. There are 2 possible reasons for this. First, it may be related to reduced protein stability due to an altered N-terminus. Such a mechanism was previously described by Tian et al in their study of the *TBCE* frameshift variant c.66_67del (12). Second, translation initiation at the reference ATG codon can lead to competition for binding to the ribosome, resulting in decreased translation initiation efficiency at downstream alternative ATG codons. Thus, the main *TBCE* ORF, being out-of-frame, overlaps with the alternative ORF and can thereby prevent its translation.

To further assess the contribution of these phenomena to the low protein expression from the +1 ORF, we created additional luciferase constructs. To investigate the influence of the reference ORF translation on the translation of the +1 ORF, we replaced the main ATG start codon with TTG in plasmids that translate luciferase from frame +1 (main) and +2 (which produces a truncated TBCE protein). This mutation prevents translation of the main ORF. We performed luciferase experiments with these new plasmids. As expected, translation of the main ORF decreased dramatically after its ATG was removed (adjusted *P*-value < .0001), while the translation level of the +1ORF did not statistically significantly change expression, although there was a tendency towards a slight increase compared to the original plasmid (Fig. 3B).

To assess the contribution of protein instability (due to an altered N-terminus) to the reduced protein expression from the +1 ORF, we introduced a P2A peptide before the luciferase coding sequence (CDS) into the corresponding plasmids. P2A is a "self-cleaving" peptide that causes the separation of the N-terminus from the luciferase protein during translation, thereby negating the contribution of protein stability to luciferase activity. Using the luciferase assay, we showed that, in

the absence of the N-terminus contribution, the translation level of the +1 ORF increased up to ~16% compared to WT plasmid (Fig. 3B).

Simultaneous removal of the reference start codon and introduction of the P2A peptide in the +1 ORF led to an increase in luciferase activity up to 69% of normal level (adjusted *P*-value = .0042), confirming the role of both described mechanisms. In summary, we concluded that both the presence of the reference ORF translation and the instability of the N-terminus reduce protein expression from *TBCE* +1 ORF (Fig. 3C).

Overexpression of Mutant TBCE Protein Leads co Complete Microtubule Dissociation

Several studies have demonstrated that overexpression of a functional TBCE protein is associated with complete dissociation of the entire MT network within the cell (9, 17). Since Western blot experiments revealed the presence of low amounts of a shortened TBCE protein in the fibroblast culture of patient 1, who is homozygous for the c.100 + 1G > A variant, we decided to perform an overexpression experiment with GFP-tagged TBCE to explore whether the mutant TBCE protein remains functional.

To do this, the CDS of both WT and mutant *TBCE* were amplified from control and patient cDNA, respectively, and cloned into the pcDNA3.1 expression vector. Consistent with previous results, overexpression of WT GFP-tagged TBCE showed complete disruption of MT in HeLa cells (Fig. 4). Similar results were observed with the mutant TBCE, indicating that the mutant protein retains functionality (Fig. 4). In contrast, *TBCE* CDS lacking exon 3 did not affect the cell MT network, indicating that this *TBCE* isoform lacks functional activity (Fig. 4). Surprisingly, overexpression of *TBCE* CDS where we introduced the previously reported in-frame deletion c.155_166del found in homozygous state in HRD patients showed complete disruption of MT network in HeLa cells (Fig. 4). Presumably, this variant does not affect TBCE function rather than affect TBCE stability.

To ensure that the observed effect of different TBCE protein isoforms on microtubule dissociation was not affected by the attachment of GFP to the N-end, the same overexpression experiments were repeated with a FLAG-tag on the protein's C-end. We observed identical results, ruling out the possible bias introduced by the fused protein (Supplementary Fig. S5) (13).

TBCE c.100 + 1G > A Homozygous Variant Does Not Affect Microtubules Architecture, Growth Rate, or Nucleation Frequency in Fibroblasts

The previously reported effects of *TBCE* homozygous and compound heterozygous pathogenic variants included the loss of microtubule network polarity and a qualitative delay in the process of microtubule regrowth after their disruption (10, 11). However, immunofluorescent staining of α-tubulin in fibroblasts from patient 1 did not reveal any morphological differences in the architecture of the microtubule system compared to control fibroblasts (Fig. 5A). Subsequently, we performed microtubule repolymerization experiments followed by careful quantitative and statistical analysis to evaluate possible changes in microtubule growth dynamics.

Based on previous data, microtubule regrowth delay was expected in patient cells. Surprisingly, the microtubule repolymerization assay did not reveal any statistically significant differences in microtubule nucleation frequency or their growth rate between patient 1 and control fibroblasts (Fig. 5A). Both control and patient fibroblasts exhibited abundant microtubule nucleation in the cytoplasm (Fig. 5B and 5C) and at the centrosome (Supplementary Fig. S7) (13) as early as 1.5 minutes after microtubule-disrupting agent washout, with subsequent microtubule growth observed at 2.5 minutes.

For quantitative analysis of microtubule nucleation frequency and their growth rate, we estimated the total number and length of free cytoplasmic microtubules, as well as the area of centrosomal microtubule asters. Statistical analysis of the length distribution of short cytoplasmic microtubules at the 1.5-minute stage of microtubule recovery showed no significant differences between patient and control fibroblasts (1631 and 1768 microtubules measured from 10 control and 10 patient cells, respectively) (Fig. 5B). This indicates the same growth rate of microtubules nucleated in the cytoplasm of both patient 1 and control fibroblasts. The number of cytoplasmic microtubules that appeared 1.5 minutes after nocodazole washout (equal to the number of cytoplasmic nucleation sites) also did not differ between control and patient fibroblasts (Fig. 5C). Similarly, the measured area of centrosomal microtubule asters did not demonstrate statistically significant differences between patient 1 and control samples (Supplementary Fig. S7) (13), which was expected given that the disruption of centrosome functional activity leads to mitosis defects and the inability to develop viable organisms from such cells.

Altogether, our results indicate that the dynamics of microtubule polymerization and the architecture of microtubules are not significantly affected in the fibroblasts of patient 1. This suggests that the homozygous c.100 + 1G > A variant does not lead to the loss of TBCE function as an α-tubulin chaperone in agreement with the overexpression data.

Golgi Compactness Suffers in Both Homozygous and Heterozygous Carriers of the c.100 + 1G > A Variant

The compactness of the Golgi apparatus directly depends on microtubule-based transport and the overall architecture of the microtubule system. Since Golgi fragmentation due to homozygous pathogenic variants in the *TBCE* gene has been previously demonstrated (11, 18), we decided to evaluate the effect of the c.100 + 1G > A *TBCE* variant on Golgi morphology.

The Golgi ribbon is a complex organelle consisting of several compartments, each containing specific protein markers on its surfaces. For a precise description of Golgi morphology, we used immunofluorescent staining with antibodies against 2 different proteins localized on the cis-Golgi membranes, GM130 and AKAP450, considering an object to be Golgi when both markers were detected. Golgi compactness was estimated as the ratio of the sum of the areas of all Golgi elements of the cell to the square of the sum of their perimeters multiplied by 4π (19).

Although we did not find significant differences in the architecture of microtubules and their growth rate in cells with the c.100 + 1G > A *TBCE* variant (as described earlier), we observed a significant loss of Golgi compactness in patient 1's fibroblasts compared to control cells (Supplementary Fig. S6) (13), consistent with previously reported data (10, 11).

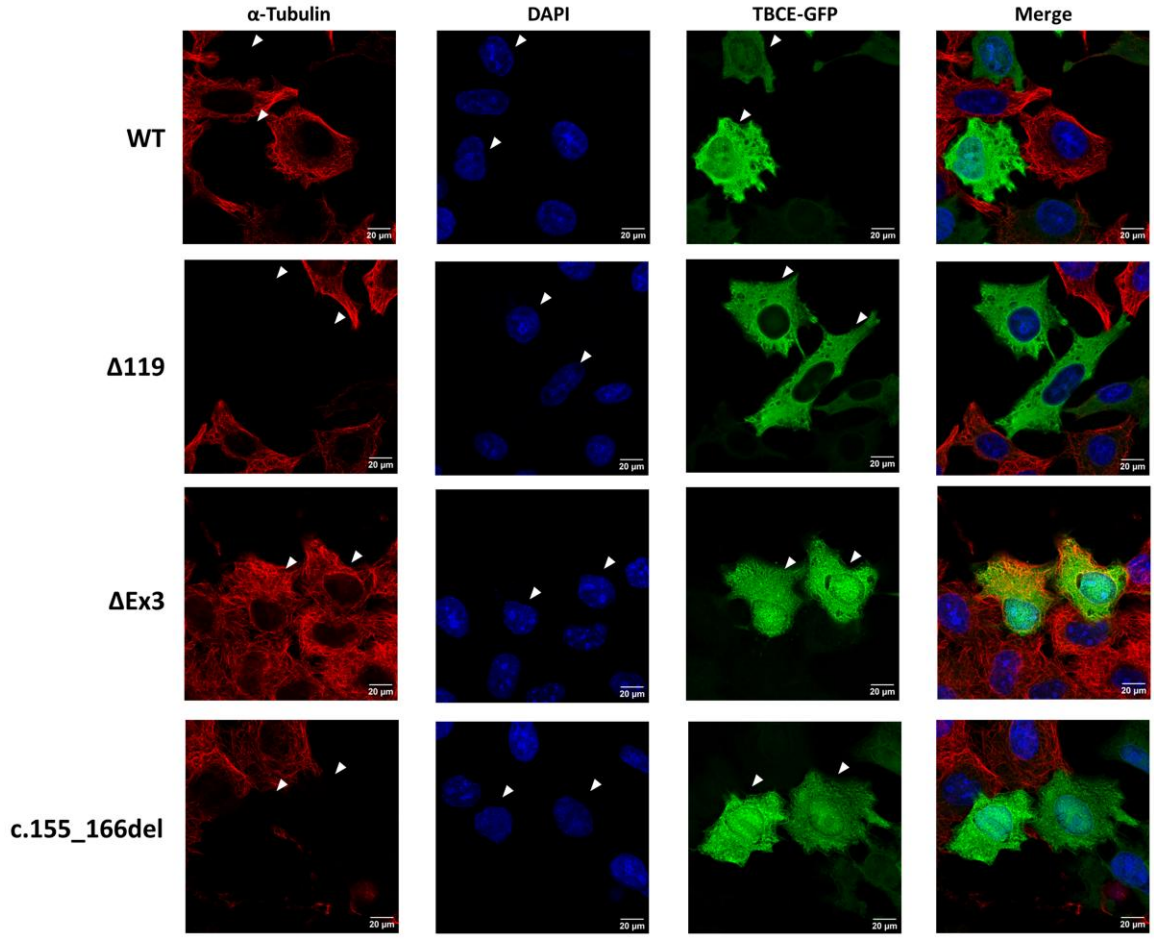

Figure 4. Mutant TBCE protein translated from the c.100 + 1G > A allele retains microtubule depolymerization activity in vivo. Confocal microscopy images of HeLa cells overexpressing N-end fused GFP-wild-type TBCE, mutant protein translated from the c.100 + 1G > A allele (Δ119), TBCE lacking exon 3 (ΔEx3), and mutant TBCE described in hypoparathyroidism-retardation-dysmorphism patients with the c.155_166del variant in a homozygous state. α-Tubulin (red, left column) and the overexpressed GFP-fused TBCE proteins (green, third column) are shown. Nuclei (blue, second column) are stained with 4′,6-diamidino-2-phenylindole. The right column shows merged images. White arrows indicate TBCE-overexpressing cells.

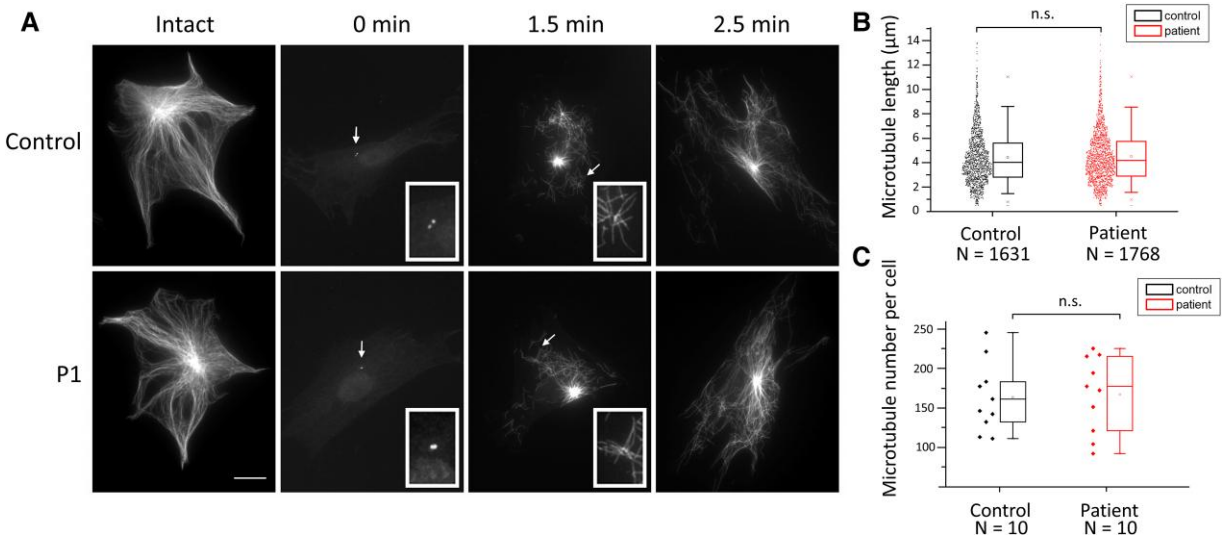

Figure 5. Mutant TBCE protein translated from the c.100 + 1G > A allele does not affect microtubule architecture, growth rate, or nucleation frequency. (A) Immunofluorescence analysis of microtubule repolymerization in control (upper panel) and patient 1 (lower panel) fibroblasts labeled for α-Tubulin after nocodazole treatment at different time points. (B) Comparison of microtubule length in control and patient 1 fibroblasts labeled for α-Tubulin at the 1.5-minute stage. (C) Comparison of microtubule number per cell in control and patient 1 fibroblasts labeled for α-Tubulin at the 1.5-minute stage.

Abbreviation: n.s., $P > .05$ by Mann-Whitney U test.

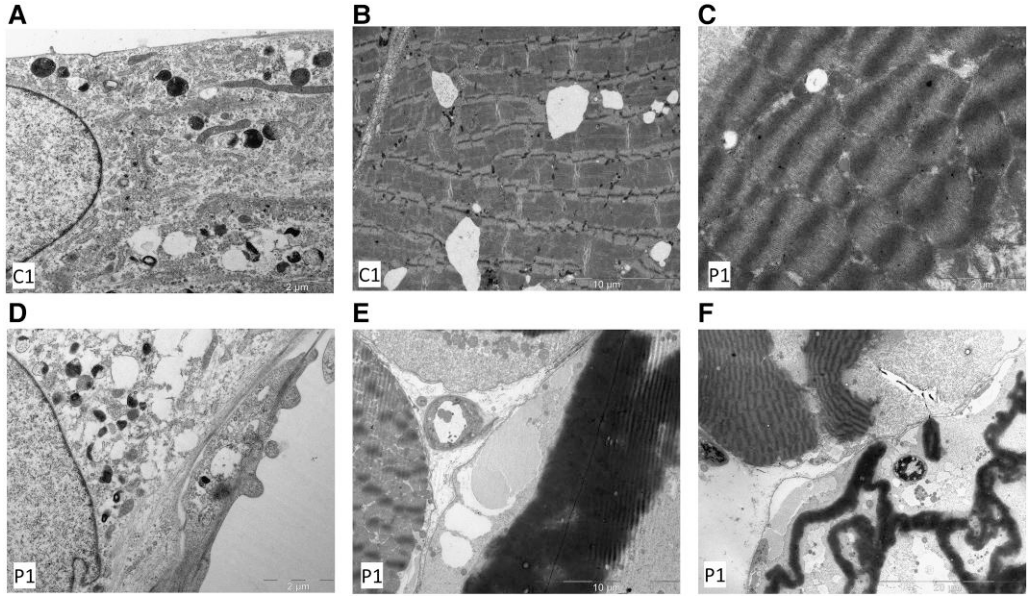

Figure 6. Ultrastructural analysis of skin fibroblast and striated muscles in a patient with the homozygous c.100 + 1G > A variant in the *TBCE* gene. Example of electron microscopy of control fibroblasts (A) and muscle samples (B) with normal ultrastructural organization. Patient 1 fibroblast (D) shows an increased amount of electrolucent vacuoles. (C, E, F) Electron microscopy of patient 1 muscle samples showing varying levels of actomyosin cytoskeleton degradation (details in text).

Moreover, Golgi compactness in the fibroblasts of the patient's mother was also significantly lower than in control cells, despite her being heterozygous for the c.100 + 1G > A *TBCE* variant. The value of this parameter did not significantly differ between the patient's and his mother's fibroblasts (Supplementary Fig. S6) (13). This suggests potential defects in intracellular transport along microtubules in cells where the c.100 + 1G > A *TBCE* variant is present, even in a heterozygous state.

Homozygous *TBCE* c.100 + 1G > A Variant Does Not Reduce Fibroblast Motility

Microtubule dynamics and transport along microtubules could determine not only Golgi morphology but also important processes such as cell motility. Our data, on one hand, indicate that the studied *TBCE* variant does not affect the architecture and dynamics of microtubules in the patient's cells (Fig. 5A-5C). However, the observed differences in Golgi morphology may suggest changes in transport along microtubules (Supplementary Fig. S6) (13), which could potentially impact cell motility. Therefore, we decided to study the parameters of locomotion in cultured primary fibroblasts from the patient and his mother and compare them with control cells.

We continuously recorded the movement of fibroblasts along the substrate in a sparse monolayer for 16 hours and subsequently analyzed their movement parameters. It was found that the average speed of movement of the mother's cells (heterozygous for the c.100 + 1G > A variant) was slightly higher than that of the patient cells (homozygous for the c.100 + 1G > A variant) (Supplementary Files 4 and 5) (13). However, no significant differences were observed between control and patient cells (Supplementary Files 3 and 5) (13) or between control and mother cells (Supplementary Files 3 and 4, Supplementary Fig. S11) (13). Thus, we can conclude that the c.100 + 1G > A variant does not significantly affect cell motility, and any observed differences may be attributable to individual variability.

Homozygous c.100 + 1G > A Variant Leads to Severe Mosaic Disorders in Ultrastructure of Striated Muscles

Next, we compared control cells and patients' cells at the ultrastructural level. We analyzed the ultrastructure of control and patient 1 fibroblasts using a transmission electron microscope. Given that the patient's phenotype includes pronounced muscular dystrophy, we also analyzed and compared ultrathin sections of his striated muscles with control samples.

As expected, the comparison of fibroblast ultrastructure did not reveal significant differences between patient and control cells: the general morphology of nuclei and various cytoplasmic organelles was largely similar (Fig. 6A and 6D). However, in patient 1's cells, we observed an increased number of large electrolucent vacuoles, similar to those observed in the ultrastructural images of HRD patients (10).

A completely different situation was found in skeletal muscle tissue. Ultrathin sections of patient 1's striated muscle fibers showed striking sarcomere heterogeneity. About a third of the sarcomeres were indistinguishable from the control, exhibiting the ultrastructure of the actomyosin system characteristic of healthy muscle fibers. In contrast, the remaining sarcomeres demonstrated significant and alarming degradation of the actomyosin cytoskeleton, up to complete destruction (Fig. 6C, 6E-6F). Sarcomeres with such ultrastructural abnormalities have obviously lost their functional activity. Thus, in the skeletal muscles of a patient homozygous for the c.100 + 1G > A variant, a pronounced mosaic pattern is observed, with most muscle fibers in the striated muscles at various stages of degradation at any given time. The presence of normal or near-normal muscle fibers suggests an ongoing regeneration process.

Alongside the distorted myofibers, abnormally structured nuclei were observed. These nuclei are characterized by the almost complete detachment of heterochromatin from the nuclear envelope (Supplementary Fig. S8) (13). The sparse remaining connections are maintained by irregularly spaced, barely visible thin chromatin threads linking heterochromatin to the inner nuclear membrane. The rest of the nucleoplasm is electron-lucent and filled with even finer fibers of unidentified origin. Some heterochromatin blocks are located in the central part of the nucleus and in association with the nucleolus. Nuclear pore complexes are evenly spaced in the nuclear envelope.

In the nuclei of healthy muscle cells, the heterochromatin maintains a very tight attachment to the inner nuclear membrane, except in the zones occupied by nuclear pore complexes. Chromatin threads fill the nucleoplasm. Some blebbing of the outer nuclear membrane was observed in both patient and control biopsies.

Discussion

Even with the introduction of comprehensive NGS-based diagnostics such as gene panels WES and whole-genome sequencing into routine clinical practice, the utility of DNA diagnostics overall remains low (20, 21). One reason is the difficulty in interpreting noncoding variants without supporting functional data. Additionally, causative variants might be filtered out due to low phenotypic similarity with previously published cases. Patient 1 underwent a diagnostic odyssey, involving counseling with several clinical geneticists, more than a dozen different genetic tests, and multiple reanalyses of WES data before the discovery of the c.100 + 1G > A variant in the *TBCE* gene. This variant, despite being a LoF variant in a homozygous state, was not reported multiple times for this very reason. Moreover, the c.100 + 1G > A variant in ClinVar is reported as having conflicting classifications of pathogenicity (Accession: VCV000631595.20) due to a lack of functional confirmation and association with a known *TBCE*-related phenotype. This variant was even reported in a homozygous state in a large cohort of patients with disorders of sex development (22). Analyzing the available clinical data, we observed similarities with our patient, including short stature, testicular abnormalities, impaired spermatogenesis, dysmorphic features, and cognitive impairment. However, the authors did not discuss the striking differences between their patient and reported *TBCE* phenotypes. According to gnomAD v4.1.0, the c.100 + 1G > A variant in the *TBCE* gene was found in a heterozygous state 109 times, mostly in people of European ancestry with an allele frequency of ≈0.001%. However, in a similar population database of controls from Russia, this variant has a 10-fold higher frequency, making it a common pathogenic variant. Most likely additional cases of this clinically recognizable phenotype remain undiagnosed due to lack of phenotypic overlap with known *TBCE*-related disorders. It is possible that similar cases involving other genes remain undiagnosed due to strict prioritization based on reported phenotypic data.

Here, using detailed clinical phenotyping and a variety of molecular methods, we decipher the molecular mechanism underlying this unique phenotype in a large clinically homogeneous cohort. Although the c.100 + 1G > A variant indeed affects splicing, leading to a presumably complete LoF of the TBCE protein, we observed a relatively mild phenotype compared with what was previously published. We show that the underlying mechanism is related to cryptic translation from downstream out-of-frame ATG codons. This, in turn, restores the reading frame starting from exon 4 of the *TBCE* gene, producing a low amount of an N-end altered yet functional protein. Examples where a canonical splice variant does not lead to a LoF effect are known (23). However, here on the RNA level, the c.100 + 1G > A variant indeed leads to a LoF effect. Classification of this variant without additional experiments on the protein level would lead to a false classification of the variant as truly LoF, thus leading to inconsistent phenotype-genotype correlation. We demonstrate here that such cases require elusive molecular investigation, which is both difficult and time-consuming, in order to eliminate the discrepancy between the observed clinical phenotype and the genetic alteration. Interestingly, the RT-PCR analysis of the c.100 + 1G > A variant demonstrated along with an activation of a cryptic donor splice-site in exon 2 skipping of exon 3. To the best of our knowledge, such examples are extremely rare if not unique given that the donor site of exon 2 and exon 3 are located more than 20 kb apart. Presumably, the 3′ end of exon 2 contains a splicing enhancer positively regulating exon 3 inclusion and loss of the enhancer due to shortening of exon 2 leads to complete skipping that is observed in patients' samples.

TBCE is an essential protein, and its complete absence is presumably embryonically lethal; as in all reported *TBCE*-related phenotypes, a residual amount of the protein was detected. All 3 downstream out-of-frame ATG codons are evolutionarily conserved across mammals and presumably also have similar translation potential as in humans. Such out-of-frame translation, as demonstrated here, may serve as a regulatory buffer that helps bypass early frameshifting variants and rescues the production of essential proteins that would otherwise be nonfunctional. Translation initiation at downstream in-frame ATG and non-ATG codons is a known phenomenon (24, 25) that can influence both disease severity and penetrance (26, 27). Taking this into consideration, the ClinGen Sequence Variant Interpretation Workgroup even recommends reducing the strength of the PVS1 criteria for start-loss variants (28). However, the extent to which out-of-frame translation can affect disease variability and penetrance genome-wide is unknown.

The patient cohort reported here is very homogeneous both clinically and genetically. Five out of 7 patients are homozygous for the c.100 + 1G > A variant and display a remarkably similar phenotype (Fig. 1A-1F). The only patient in the cohort with a relatively more severe phenotype is patient 6, who is compound heterozygous, carrying the c.101G > T missense variant on the other allele. We demonstrated that this variant partially affects splicing, leading to skipping of exon 3. This, in turn, causes a frameshift where no alternative translation occurs, and NMD is activated. Deep sequencing revealed that in patient 6, only 2.1% of reads correspond to the full-length isoform with a missense variant located in the CAP-Gly domain. Overall, the even more pronounced reduction in TBCE level in patient 6, as shown by Western blot, is responsible for his more severe clinical outcome. Interestingly, patient 3, who is also compound heterozygous (c.100 + 1G > A/c.512T > A), showed great similarity to other patients (Fig. 1A and 1D). This missense variant is located in the LRR1 repeat of the TBCE protein, where the p.Ile155Asn variant was previously described in the progressive

encephalopathy with amyotrophy and optic atrophy phenotype (11). In the original paper, the authors concluded that this variant is hypomorphic, which explains the less severe phenotype in their cohort. Although we did not analyze the effect of the c.512T > A variant due to the lack of patient-derived samples, we believe that the effect of this variant on protein function is even less marked, leading to our novel mild phenotype.

Overexpression analysis proved that the mutant TBCE protein translated from the mutant allele in our patients is able to disassemble the MT network and is therefore functional. Unexpectedly, when testing the in-frame deletion reported in patients with HRD, we also observed that the mutant protein completely disrupted the MT network. These results suggest that the c.155_166del deletion manifests in an alternative manner rather than affecting TBCE function, possibly by decreasing TBCE stability. In the only clinical report providing Western blot data from an HRD patient, the amount of TBCE was negligible, confirming this hypothesis (29).

The initial report demonstrating the possibility of cryptic out-of-frame translation in the *TBCE* gene showed that, similarly, the mutant TBCE protein translated from the c.66_67del allele is functional. Although this protein also has an altered N-end, which is most likely responsible for increased sensitivity to proteolysis and consequently low protein stability, the CAP-Gly domain is completely preserved. In contrast, the mutant protein translated from the c.100 + 1G > A allele contains only the last 10 amino acids of the CAP-Gly domain, yet it remains functional. In the work by Serna et al, several deletion constructs were analyzed to narrow down the functional core region of the TBCE protein (17). Similar overexpression analysis demonstrated that, in a TBCE protein completely lacking the CAP-Gly domain, the microtubule depolymerization activity is abolished. The CAP-Gly deletion construct had an 83-amino-acid deletion starting from the first residue at the N-end of the protein. Such a protein not only lacks the CAP-Gly domain, which is mapped to residues 27-71, but also the entire N-end of the protein, potentially preventing proper folding into its native 3-dimensional conformation. This suggests that it is not the absence of the CAP-Gly domain that disrupts TBCE function. Alternatively, it is possible that the last 10 amino acids present in the mutant protein of our patients are sufficient to drive tubulin interaction or that the CAP-Gly domain is redundant in terms of MT disassembly and is not essential for the association of the TBCD-TBCE-TBCC-αβ-tubulin complex and hence for the formation of αβ-tubulin heterodimers. This assumption does not contradict previously published structural data on the core tubulin chaperone consisting of tubulin cofactors TBCD, TBCE, and Arl2, where deletion of the CAP-Gly domain did not affect the assembly of soluble TBC-DEG complexes (6).

In a previous study on the effect of *TBCE* LoF variants in motor neurons leading to Golgi fragmentation, the authors concluded that Golgi vesiculation in TBCE-depleted cells was due to a reduction in nucleation and growth of Golgi-derived microtubules (18). However, our data did not reveal any deviations in noncentrosomal microtubule nucleation and growth dynamics in patient 1's fibroblasts with the homozygous c.100 + 1G > A *TBCE* variant, although we did detect a loss of Golgi compactness in his cells. The reason for these changes needs further clarification.

Comparison of our patients to those with HRD/Kenny-Caffey syndrome type 1 and the progressive encephalopathy with amyotrophy and optic atrophy phenotype clearly shows that the novel phenotype is less severe (Table 1). At the molecular level, the severe phenotype of HRD/Kenny-Caffey syndrome type 1 is most likely related to the pronounced reduction in TBCE protein. In the progressive encephalopathy with amyotrophy and optic atrophy phenotype, the protein level was not reduced, but its function was altered, as demonstrated by the reduced repolymerization of microtubules in such patients. In contrast, our findings clearly show a less pronounced reduction in TBCE levels, as evidenced by Western blot. Moreover, the protein remains functional, as shown by both normal repolymerization rates and overexpression experiments, thus explaining the relatively mild phenotype of our patients.

When quantifying the translation efficiency of the out-of-frame ATG codons for the first time using the luciferase assay, we observed that the translation efficiency is only 4% compared with the reference ATG. This partially contradicts the Western blot results from patient 1 fibroblasts, where we found a reduced level of a shortened protein but to a lesser degree. The extremely low translation efficiency observed in the luciferase assay may be biased by both the artificial reduction of the genomic background introduced into the plasmid, which may lack important regulatory sequences, and by cell-line specific effects observed in HEK293T cells. Future research quantifying translation efficiency in different cell lines may resolve this inconsistency. The presence of a tissue-specific effect on TBCE abundance is confirmed by the Western blot data from the muscle sample of patient 1, where we observed a lower TBCE level compared with skin fibroblasts (Supplementary Fig. S3) (13). This correlates with the observation of more severe involvement in skeletal muscles in our patients.

The experiments conducted in this study primarily address the effect of the c.100 + 1G > A variant at the molecular and cellular levels. Although we showed that the splice variant results in disruption of mRNA and protein structure, it seems that the main molecular effect is a decrease in TBCE expression. However, how these alterations ultimately lead to the observed phenotype at the pathophysiological level remains unclear. We hypothesize that the primary mechanism involves microtubule-related organelle dysfunction, particularly within the Golgi complex, ultimately leading to apoptosis. Nevertheless, given that TBCE is ubiquitously expressed across most tissues, why the TBCE dysfunction caused by the c.100 + 1G > A variant predominantly affects endocrine organs and muscle tissue remains a subject for future research.

Overall, detailed clinical and molecular phenotyping revealed a novel mild *TBCE*-related phenotype in a patient cohort of Slavic origin, all sharing the c.100 + 1G > A variant in a homozygous or compound heterozygous state. This variant leads to splicing alteration and an early frameshift. However, we demonstrated that cryptic translation from out-of-frame ATG codons restores the reading frame and rescues the production of a shortened, N-end-altered TBCE protein that remains functional. The mutant protein is translated at a reduced level due to both competition with the reference ATG codon by the ribosome and reduced stability of the protein owing to its modified N-end. Nevertheless, even the reduced amount is sufficient to lead to a unique phenotype that we named amyotrophy, testicular failure, and mild

intellectual disability with or without short stature based on its main clinical features. Our work uncovers insight on a unique mechanism of phenotypic rescue of an early frameshifting variant that can serve as a blueprint for similar work in other genes, offering explanations for the molecular mechanisms of varying expressivity and incomplete penetrance.

Acknowledgments

We would like to acknowledge the individuals and families involved in this study.

Funding

This work was supported by The Ministry of Science and Higher Education of the Russian Federation (the Federal Scientific-technical programme for genetic technologies development for 2019-2030, agreement № 075-15-2021-1061, RF 193021X0029).

Author Contributions

P.S. performed RT-PCR analysis, analyzed the data, curated patients 1 and 3, and wrote the manuscript draft. E.U. performed Western blot experiments, microtubule repolymerization assay, and Golgi compactness analysis and analyzed the data. A.F. performed the luciferase assay and analyzed the data. E.T. conducted immunofluorescence experiments and overexpression assay and analyzed the data. G.P. performed immunofluorescence analysis of Golgi complex compactness. M.N., E.N., M.K., E.F., N.K., V.V., and A.T. collected the patient's cohort and analyzed the clinical data. A.Tv. performed confocal microscopy and analyzed the data. S.G. conducted electron microscopy experiments. A.B. conducted the fibroblast motility assay. V.K. obtained cell cultures and analyzed the data. E.L and F.K. performed bioinformatic analysis. M.S. cloned expression and lucifarse plasmids and supervised the project. P.S., V.V., A.T., and M.S. conceptualized the project. All authors reviewed and contributed to revising and editing the manuscript draft.

Disclosures

The authors have nothing to declare.

Data Availability

All data needed to evaluate the conclusions in the paper are present in the paper and/or the Supplementary Material. All additional data are available from the corresponding authors upon reasonable request.

Patient Consent for Publication

All research participants gave written informed consent (or responsible consent form for infant proband) to the clinical examination and the publication of their anonymized data.

Ethics Approval

The study was performed in accordance with the Declaration of Helsinki and approved by the Institutional Review Board of the Research Centre for Medical Genetics, Russia.

References

1. Brouhard GJ, Rice LM. Microtubule dynamics: an interplay of biochemistry and mechanics. *Nat Rev Mol Cell Biol*. 2018;19(7):451-463.
2. Redemann S, Furthauer S, Shelley M, Muller-Reichert T. Current approaches for the analysis of spindle organization. *Curr Opin Struct Biol*. 2019;58:269-277.
3. Kaverina I, Straube A. Regulation of cell migration by dynamic microtubules. *Semin Cell Dev Biol*. 2011;22(9):968-974.
4. Mitchison T, Kirschner M. Dynamic instability of microtubule growth. *Nature*. 1984;312(5991):237-242.
5. Lundin VF, Leroux MR, Stirling PC. Quality control of cytoskeletal proteins and human disease. *Trends Biochem Sci*. 2010;35(5):288-297.
6. Nithianantham S, Le S, Seto E, *et al*. Tubulin cofactors and Arl2 are cage-like chaperones that regulate the soluble alphabeta-tubulin pool for microtubule dynamics. *Elife*. 2015;4:e08811.
7. Tian G, Lewis SA, Feierbach B, *et al*. Tubulin subunits exist in an activated conformational state generated and maintained by protein cofactors. *J Cell Biol*. 1997;138(4):821-832.
8. Tian G, Bhamidipati A, Cowan NJ, Lewis SA. Tubulin folding cofactors as GTPase-activating proteins. GTP hydrolysis and the assembly of the alpha/beta-tubulin heterodimer. *J Biol Chem*. 1999;274(34):24054-24058.
9. Kortazar D, Carranza G, Bellido J, Villegas JC, Fanarraga ML, Zabala JC. Native tubulin-folding cofactor E purified from baculovirus-infected sf9 cells dissociates tubulin dimers. *Protein Expr Purif*. 2006;49(2):196-202.
10. Parvari R, Hershkovitz E, Grossman N, *et al*. Mutation of TBCE causes hypoparathyroidism-retardation-dysmorphism and autosomal recessive kenny-caffey syndrome. *Nat Genet*. 2002;32(3):448-452.
11. Sferra A, Baillat G, Rizza T, *et al*. TBCE mutations cause early-onset progressive encephalopathy with distal spinal muscular atrophy. *Am J Hum Genet*. 2016;99(4):974-983.
12. Tian G, Huang MC, Parvari R, Diaz GA, Cowan NJ. Cryptic out-of-frame translational initiation of TBCE rescues tubulin formation in compound heterozygous HRD. *Proc Natl Acad Sci U S A*. 2006;103(36):13491-13496.
13. Sparber P. Supplementary materials. *Zenodo*. http://doi.org/10.5281/zenodo.14176425. Deposited 17 November 2024.
14. Richards S, Aziz N, Bale S, *et al*. Standards and guidelines for the interpretation of sequence variants: a joint consensus recommendation of the American College of Medical Genetics and Genomics and the Association for Molecular Pathology. *Genet Med*. 2015;17(5):405-424.
15. Helbig KL, Farwell Hagman KD, Shinde DN, *et al*. Diagnostic exome sequencing provides a molecular diagnosis for a significant proportion of patients with epilepsy. *Genet Med*. 2016;18(9):898-905.
16. Sparber P, Mikhaylova S, Galkina V, Itkis Y, Skoblov M. Case report: functional investigation of an undescribed missense variant affecting splicing in a patient with dravet syndrome. *Front Neurol*. 2021;12:761892.
17. Serna M, Carranza G, Martin-Benito J, *et al*. The structure of the complex between alpha-tubulin, TBCE and TBCB reveals a tubulin dimer dissociation mechanism. *J Cell Sci*. 2015;128(9):1824-1834.
18. Bellouze S, Schafer MK, Buttigieg D, Baillat G, Rabouille C, Haase G. Golgi fragmentation in pmn mice is due to a defective ARF1/TBCE cross-talk that coordinates COPI vesicle formation and tubulin polymerization. *Hum Mol Genet*. 2014;23(22):5961-5975.
19. Kucherov AL. Status and prospects of the development of antituberculosis services in the RSFSR. *Probl Tuberk*. 1988;(7):3-5.
20. Alfares A, Aloraini T, Subaie LA, *et al*. Whole-genome sequencing offers additional but limited clinical utility compared with reanalysis of whole-exome sequencing. *Genet Med*. 2018;20(11):1328-1333.

21. Bagger FO, Borgwardt L, Jespersen AS, *et al.* Whole genome sequencing in clinical practice. *BMC Med Genomics*. 2024;17(1):39.
22. Globa E, Zelinska N, Shcherbak Y, Bignon-Topalovic J, Bashamboo A, Msmall es CK. Disorders of sex development in a large Ukrainian cohort: clinical diversity and genetic findings. *Front Endocrinol (Lausanne)*. 2022;13:810782.
23. Lin JH, Tang XY, Boulling A, *et al.* First estimate of the scale of canonical 5′ splice site GT > GC variants capable of generating wild-type transcripts. *Hum Mutat*. 2019;40(10):1856-1873.
24. Bazykin GA, Kochetov AV. Alternative translation start sites are conserved in eukaryotic genomes. *Nucleic Acids Res*. 2011;39(2):567-577.
25. Na CH, Barbhuiya MA, Kim MS, *et al.* Discovery of noncanonical translation initiation sites through mass spectrometric analysis of protein N termini. *Genome Res*. 2018;28(1):25-36.
26. Hasey GM, Stancer HC, Warsh JJ, Persad E. Neurotransmitter metabolites and endocrine responses in depression. *Prog Neuropsychopharmacol Biol Psychiatry*. 1985;9(5-6):613-617.
27. Starck SR, Jiang V, Pavon-Eternod M, *et al.* Leucine-tRNA initiates at CUG start codons for protein synthesis and presentation by MHC class I. *Science*. 2012;336(6089):1719-1723.
28. Abou Tayoun AN, Pesaran T, DiStefano MT, *et al.* ClinGen sequence variant interpretation working G. Recommendations for interpreting the loss of function PVS1 ACMG/AMP variant criterion. *Hum Mutat*. 2018;39(11):1517-1524.
29. Courtens W, Wuyts W, Poot M, *et al.* Hypoparathyroidism-retardation-dysmorphism syndrome in a girl: a new variant not caused by a TBCE mutation–clinical report and review. *Am J Med Genet A*. 2006;140(6):611-617.